



Pergamon

## 3-D-QSAR Study and Molecular Docking of Methionyl-tRNA Synthetase Inhibitors

Su Yeon Kim and Jeewoo Lee\*

Laboratory of Medicinal Chemistry, Research Institute of Pharmaceutical Sciences, College of Pharmacy,  
Seoul National University, Shinlim-Dong, Kwanak-Ku, Seoul 151-742, South Korea

Received 17 July 2003; accepted 29 September 2003

**Abstract**—The three-dimensional quantitative structure–activity relationships of 57 2-[(aminopropyl)amino]-4(1H)-quinolinone analogues as *Staphylococcus aureus* methionyl-tRNA synthetase (MetRS) inhibitors with excellent antibacterial profile were investigated and docking studies were performed. The CoMFA analysis provided a model with a  $q^2$  value of 0.579 and an  $r^2$  value of 0.970, in which the good correlation between the MetRS inhibitory activities ( $IC_{50}$ ) and the steric and electrostatic molecular fields around the analogues was examined. Two inhibitors (**1** and **17**) were docked into the binding pocket of *Escherichia coli* MetRS imported from the X-ray crystal structure of the MetRS-methionine complex, and the details of their interaction with the amino acids of the active site are discussed.

© 2003 Elsevier Ltd. All rights reserved.

### Introduction

The growing resistance to mainstream antibiotics has become a serious and unsettled problem in medical treatment. In particular, two prominent Gram-positive strains, methicillin resistant *Staphylococcus aureus* (MRSA) and vancomycin resistant *enterococci* (VRE), are fatal pathogens because of their resistance to all clinical antibiotics.<sup>1</sup> The urgent need for novel molecular targets has encouraged the search for new classes of antibacterial agents. For this purpose, one of the promising novel targets is the family of aminoacyl-tRNA synthetase (aaRS).<sup>2,3</sup> These enzymes catalyze the aminoacylation of a specific amino acid to its cognate tRNA, and the resulting aminoacyl-tRNAs are substrates for translation in protein synthesis and are pivotal in determining how the genetic code is interpreted as amino acids.<sup>4,5</sup> Since aaRSs are universal and essential for cell viability in all living organisms, pathogen-specific inhibition is the key issue for the clinical application of the enzyme inhibitors. Since the studies showed that pseudomonic acid selectively inhibited the bacterial isoleucyl-tRNA synthetase, without affecting the mammalian counterpart, this enzyme has been validated as an antibacterial molecular target.<sup>6</sup>

Among the inhibitors of the 20 aminoacyl-tRNA synthetases, several studies have attempted to target the bacterial methionyl-tRNA synthetase.<sup>7–15</sup> Recently, Jarvest et al. reported the discovery and structure–activity relationships of a series of 2-[(aminopropyl)amino]-4(1H)-quinolinones, as a new class of *S. aureus* methionyl-tRNA synthetase inhibitors with nanomolar  $IC_{50}$  values and potent antibacterial activities.<sup>12–14</sup> As a structure–activity relationship study of the benzyl group of the lead compound, extensive modifications of the 2-, 3- and 5-positions of the phenyl group with halogens or small and large polar substituents were described. Briefly, the unsubstituted phenyl derivative exhibited poor MetRS inhibition and thus had no antibacterial activity. Analyses of the 2-position indicated that small alkoxy groups, such as ethoxy, were optimal for increasing MetRS inhibition and the antibacterial activity. At the 3- and 5-positions, halogen and methylthio groups showed the most potent antibacterial activity.

To clarify the structural requirements of these analogues for *S. aureus* MetRS inhibition and eventually to find the ultimate inhibitor as a clinical candidate, we have investigated the three-dimensional quantitative structure–activity relationship (3-D-QSAR) by using the comparative molecular field analysis (CoMFA) method, which was originally developed by Cramer in 1988.<sup>16</sup> The principle of this method is that molecules are compared by aligning them in space and mapping their

\*Corresponding author. Tel.: +82-2-880-7846; fax: +82-2-888-0649; e-mail: jeewoo@snu.ac.kr

steric and electrostatic fields to a 3-D-grid. The correlation of the differences in these fields to their biological activities can be used to analyze the interactions between molecules and their molecular target. In this method, the potential energy fields are calculated as static, using the 6–12 Lennard–Jones potential and electrostatic using the Coulombic potential. A partial least squares (PLS) analysis of an extension of the multiple linear regression model is usually used to correlate the field values of the molecules with their biological activities and to predict the biological activities of newly designed molecules prior to synthesis. The CoMFA method has been widely applied to a number of different classes of compounds, and is now generally regarded as a useful tool for deriving 3-D-QSAR models. In this paper, we describe the 3-D-QSAR of 4-quinolinone methionyl-tRNA synthetase inhibitors using CoMFA and the docking study of potent inhibitors selected to identify the interactions between the inhibitor and the protein.

### Results and Discussion

The statistical results of the CoMFA analysis are summarized in Table 1. The resulting CoMFA analysis derived a good predictive and statistically significant model of a series of 4-quinolinone MetRS inhibitors ( $q^2=0.579$  and  $r^2=0.970$ ). The compounds **1** and **42** were included in the training set to generate the primitive QSAR model covering the widest data range of  $IC_{50}$  values from 3.0 to 300.0 nM. The cross-validated  $q^2$  is 0.309 (standard error of prediction=0.325 and optimum number of components=5), and the non-cross-validated  $r^2$  is 0.891 (standard error of estimate=0.129) for this model. The  $r^2$  of 0.891 for the model is nearly as good. However, a detailed examination of the data set was required to improve the predictability of QSAR model considerably. By the SAR result, 2,3,5-trisubstituted phenyl derivatives are preferred over dihalo analogues as potent MetRS inhibitors. In addition, the latter compounds only occupied a small portion (12%) of the total number. Based on this observation, QSAR was repeated, without the 3,5-dichloro analogue **42** ( $IC_{50}=3.0$  nM), to investigate the influence of the compound on QSAR process analysis. The QSAR model was stabilized at higher numbers of components. The optimal cross-validated  $q^2$  was improved from 0.309 to 0.579 with 8 being the optimal number of components, and the cross-validated standard error was dropped correspondingly from 0.325 to 0.264. The non-cross-validated  $r^2$  was increased from 0.891 to 0.970, which

corresponds to reducing the standard error of regression from 0.129 to 0.071. The actual and calculated  $pIC_{50}$  values for the training set are summarized in Table 2. The differences between the actual and calculated  $pIC_{50}$  values were very small (standard deviation=0.06, maximum=0.21, and minimum=-0.16). The plot of the actual versus calculated  $pIC_{50}$  values for the training set is shown in Figure 1.

To judge the predictive ability of the 3-D-QSAR model for new drug candidates, the  $pIC_{50}$  values for the test set were evaluated. The actual and predicted  $pIC_{50}$  values for the test set are summarized in Table 3. The 3,5-dichloro analogue **42** produced a large prediction error (0.78) as a test compound. All of the other dichloro derivatives have the  $IC_{50}$  value in the range of 9.0–16.0 nM, while the unique compound **42** showed a potent inhibitory activity ( $IC_{50}=3.0$  nM). The  $pIC_{50}$  value of compound **45** was predicted as 8.18. The molecular properties of compound **45** are quite similar to those of compound **17**, but the  $IC_{50}$  value of compound **45** is approximately 20 times larger than that of compound **17**. Probably, the large error in the prediction was caused by this confusion. The prediction errors for the compounds **46** and **48** were calculated as -0.70 and -1.42, respectively. The substituents at the 5-position of the aryl moiety of these compounds are large polar groups, such as  $-MeSO_2$  and  $-CO_2Et$ , which are not similar to any compounds in the training set. The compounds **50** and **57** have the pretty large hydrophobic substituents, *t*-butyl and ethyl groups, at the 3-position. Therefore, these types of interaction fields might not be trained thoroughly in the CoMFA analysis. The predicted  $pIC_{50}$  value for the six-membered ring compound **53** is 7.74 as being equal to the compound **42**. Since both compounds **42** and **53** have the same functional groups (3,5-diCl), the QSAR model estimated their activities to be equivalent. All of the other molecules in the test set were fairly well predicted.

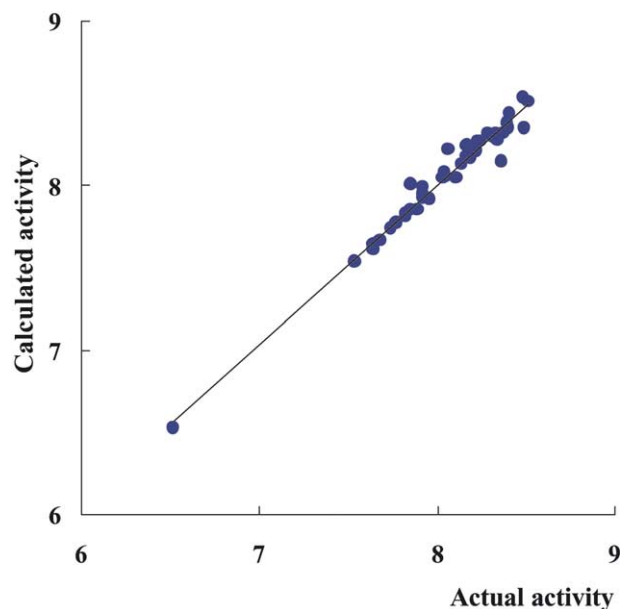


Figure 1. Actual versus calculated  $pIC_{50}$  values for the training set.

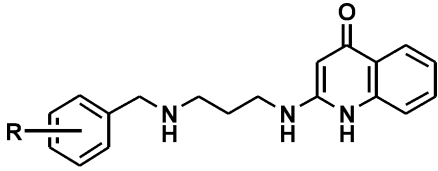
Table 1. Statistical results of the CoMFA analysis

Cross-validated $q^2$	0.579
Standard error of prediction	0.264
Optimum number of components	8
Conventional $r^2$	0.970
Standard error of estimate	0.071
F value	124.198
Field contribution	
CoMFA steric	0.492
CoMFA electrostatic	0.508

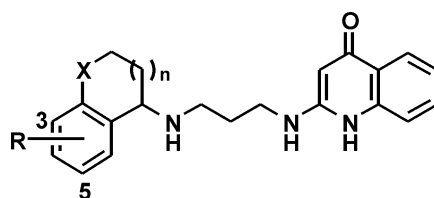
The contributions of the CoMFA steric and electrostatic interactions were 49 and 51%, respectively. The contours of the CoMFA steric and electrostatic maps are given in Figure 2. In the CoMFA steric map, sterically favored and disfavored regions are represented in green and yellow, respectively. The green contours around the substituents at the 3-position of the aryl moiety indicate that slightly bulky groups, like methyl

or halogen, enhance the MetRS inhibition. In contrast, the yellow contours enclosing the substituents at the 2- and 5-positions of the aryl moiety designate that the sterically bulky groups, such as  $-i\text{PrO}$ ,  $-\text{NHet}$  and  $-\text{MeSO}$ , attenuate MetRS inhibition. These analyses imply that the MetRS inhibitor binding sites for the 2-, 3- and 5-positions are restricted. The CoMFA electrostatic map is represented by negatively charged favored

**Table 2.** Molecular structures and enzyme inhibitory activities of 40 MetRS inhibitors constituting the training set in the QSAR analysis



Compd	R	IC <sub>50</sub> (nM)	pIC <sub>50</sub>	Calcd pIC <sub>50</sub>	Residual
1	—	300.0	6.52	6.53	−0.01
2	2,3-diCl	15.0	7.82	7.81	0.01
3	2,4-diCl	15.0	7.82	7.83	−0.01
4	2,5-diCl	9.0	8.05	8.06	−0.01
5	3,5-diI	6.4	8.19	8.17	0.02
6	2-EtO, 3,5-diCl	14.0	7.85	8.01	−0.16
7	2-AllylO, 3,5-diCl	7.2	8.14	8.13	0.01
8	2- <i>i</i> PrO, 3,5-diCl	29.0	7.54	7.54	0.00
9	2-EtO, 3,5-diBr	4.4	8.36	8.15	0.21
10	2-NH <sub>2</sub> , 3,5-diBr	9.1	8.04	8.08	−0.04
11	2-NHMe, 3,5-diBr	11.0	7.96	7.92	0.04
12	2-NH <sub>2</sub> t, 3,5-diBr	18.0	7.74	7.74	0.00
13	2-EtO, 3-Cl, 5-MeO	4.3	8.37	8.32	0.05
14	2-EtO, 3-Br, 5-I	8.8	8.06	8.22	−0.16
15	2-EtO, 3-Br, 5-Me	4.9	8.31	8.30	0.01
16	2-EtO, 3-Br, 5-CN	4.6	8.34	8.28	0.06
17	2-EtO, 3-Br, 5-MeO	3.1	8.51	8.51	0.00
18	2-EtO, 3-Br, 5-MeS	4.7	8.33	8.32	0.01
19	2-EtO, 3-Br, 5-MeSO	23.0	7.64	7.64	0.00
20	2-EtO, 3-I, 5-Br	5.9	8.23	8.27	−0.04
21	2-EtO, 3-I, 5-CH <sub>2</sub> OH	14.0	7.85	7.85	0.00
22	2-EtO, 3-I, 5-CH <sub>2</sub> OMe	17.0	7.77	7.77	0.00
23	2-EtO, 3-I, 5-MeO	3.3	8.48	8.54	−0.06
24	2-EtO, 3-MeS, 5-Br	21.0	7.68	7.67	0.01
25	2-EtO, 3-Me, 5-Cl	6.8	8.17	8.24	−0.07
26	2-EtO, 3-Me, 5-Br	5.7	8.24	8.27	−0.03
27	2-EtO, 3-Me, 5-I	3.2	8.49	8.35	0.14
28	2-EtO, 3-Me, 5-MeS	5.1	8.29	8.32	−0.03
29	2-EtO, 3-Me, 5-CN	3.9	8.41	8.44	−0.03
30	2-EtO, 3-Me, 5-CF <sub>3</sub>	6.8	8.17	8.18	−0.01
31	2-EtO, 3-CH <sub>2</sub> OH, 5-I	4.1	8.39	8.38	0.01
32	2-EtO, 3-CN, 5-Br	4.0	8.40	8.35	0.05
33	2-EtO, 3-MeO, 5-Br	13.0	7.89	7.85	0.04
34	2-EtO, 3-MeO, 5-I	12.0	7.92	7.93	−0.01



Compd	R	X	n	IC <sub>50</sub> (nM)	pIC <sub>50</sub>	Calcd pIC <sub>50</sub>	Residual
35	3,5-diCl	O	0	6.0	8.22	8.21	0.01
36	3,5-diCl	NH	1	23.0	7.64	7.61	0.03
37	3,5-diBr	O	1	7.8	8.11	8.05	0.06
38	3-Cl, 5-I	O	1	12.0	7.92	7.99	−0.07
39	3-I, 5-Cl	O	1	9.4	8.03	8.05	−0.02
40	3-I, 5-Et	NH	1	12.0	7.92	7.95	−0.03

(red) and disfavored (blue) regions. The red contours near the substituents at the 2- and 5-positions of the aryl moiety show that functional groups with high electron densities, such as halogen and small alkoxy groups, increase the MetRS inhibition. The blue contours surrounding the bulky groups at the 5-position display that the negatively charged groups decrease the MetRS inhibition. These types of interaction fields were origi-

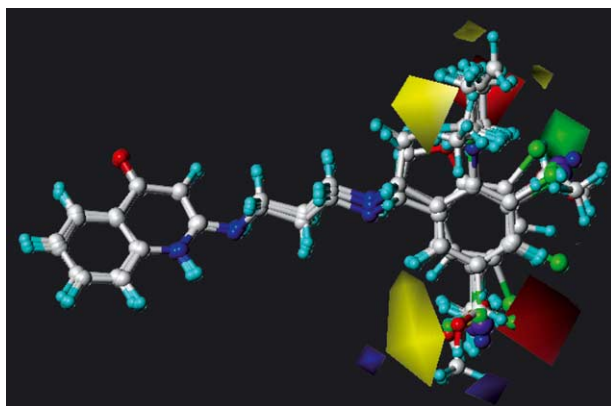


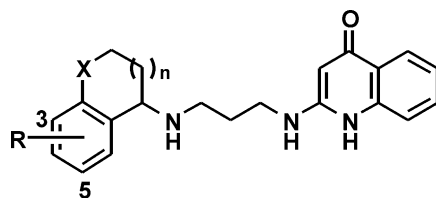
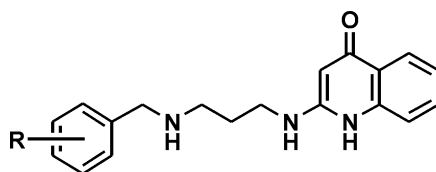
**Figure 2.** The contours of the CoMFA steric and electrostatic maps generated by  $\text{StDev} \times \text{Coeff}$ .

nated with a couple of compounds (**19** and **22**) which have the large polar groups, such as sulfone and ether. The CoMFA analysis is quite consistent with the biological activity trends of the series of MetRS inhibitors.

The resultant MetRS-compound **1** and MetRS-compound **17** complexes are shown in Figure 3b and c, respectively. The representations of the Connolly surface of the MetRS binding pocket and the spacefilling models of the analogues suggest that the enhanced potency of compound **17** resulted from its tight-binding to the pocket for the small substituents at the 2-, 3- and 5-positions of the aryl moiety. To analyze the important interactions between the MetRS binding pocket and the inhibitors, we inspected the hydrogen bond patterns summarized in Figure 4. Compound **1** forms two hydrogen bonds, with Asp296 and a water molecule, at 1.607 and 1.690 Å. In the molecule, only the hetero atoms of the quinolinone ring participate in hydrogen bonding. However, compared with that of compound **1**, the hydrogen bond pattern involved with the binding of compound **17** is more complicated. The hydrogen bonds shown in compound **1** are well conserved, and the nitrogen atom ( $\text{N}_2$ ) of an amine group and the oxygen atom of an ethoxy group form additional hydrogen bonds with water molecules, at 2.640 and 1.811 Å. The compact hydrogen bond network around compound **17**

**Table 3.** Molecular structures and enzyme inhibitory activities of 17 MetRS inhibitors constituting the test set in the QSAR analysis

Compd	R	$\text{IC}_{50}$ (nM)	$\text{pIC}_{50}$	Calcd $\text{pIC}_{50}$	Residual
<b>41</b>	3,4-diCl	16.0	7.80	7.34	0.46
<b>42</b>	3,5-diCl	3.0	8.52	7.74	0.78
<b>43</b>	3-Br, 5-I	3.2	8.49	8.02	0.47
<b>44</b>	2- $\text{CF}_3\text{CH}_2\text{O}$ , 3,5-diBr	11.0	7.96	8.05	-0.09
<b>45</b>	2-EtO, 3-Br, 5-EtO	61.0	7.21	8.18	-0.97
<b>46</b>	2-EtO, 3-Br, 5- $\text{MeSO}_2$	72.0	7.14	7.84	-0.70
<b>47</b>	2-EtO, 3-I, 5-Me	7.2	8.14	8.34	-0.20
<b>48</b>	2-EtO, 3-I, 5- $\text{CO}_2\text{Et}$	170.0	6.77	8.19	-1.42
<b>49</b>	2-EtO, 3- $\text{CH}_2\text{OMe}$ , 5-I	9.4	8.03	8.30	-0.27
<b>50</b>	2-EtO, 3- <i>t</i> Bu, 5-I	120.0	6.92	8.02	-1.10
<b>51</b>	2-EtO, 3- $\text{CO}_2\text{Et}$ , 5-I	21.0	7.68	7.79	-0.11



Compd	R	X	n	$\text{IC}_{50}$ (nM)	$\text{pIC}_{50}$	Calcd $\text{pIC}_{50}$	Residual
<b>52</b>	3,5-diCl	$\text{CH}_2$	0	5.1	8.29	8.01	0.28
<b>53</b>	3,5-diCl	$\text{CH}_2$	1	3.8	8.42	7.74	0.68
<b>54</b>	3,5-diBr	NH	1	8.0	8.10	7.66	0.44
<b>55</b>	3-Br, 5-Me	NH	1	8.0	8.10	7.94	0.16
<b>56</b>	3-Me, 5-Br	NH	1	9.4	8.03	7.69	0.34
<b>57</b>	3-Et, 5-Br	NH	1	4.3	8.37	7.34	1.03

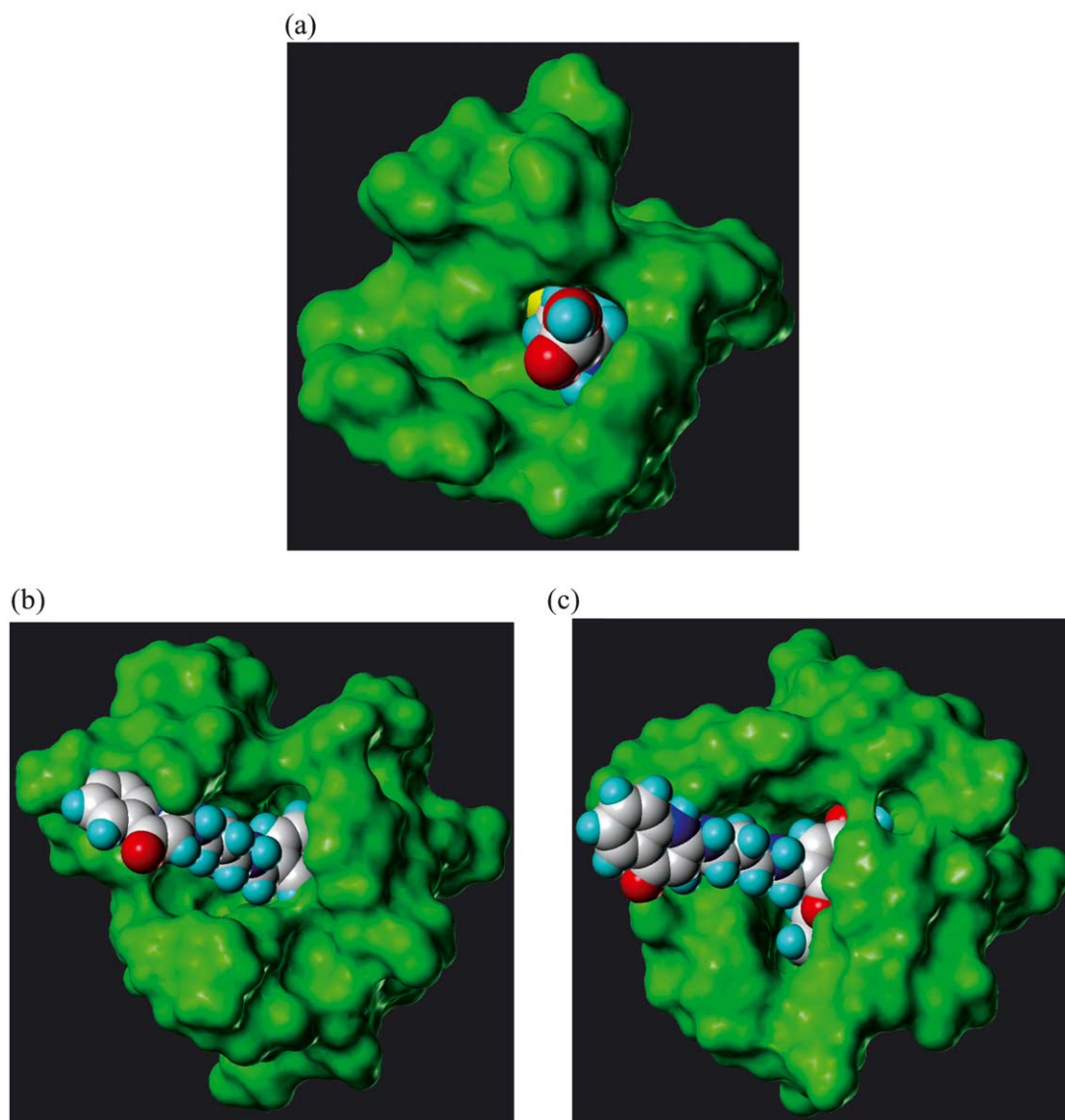


**Figure 3.** (a) The binding pocket of *E. coli* MetRS complexed with methionine; (b, c) docked models of compounds **1** and **17**, respectively, with *E. coli* MetRS.

helps to explain why this compound is more potent than compound **1**. In the MetRS-compound **17** model, both 2-EtO and 5-MeO groups are enveloped with the negatively charged amino acids, Tyr15, His24, Glu27, and Trp253. The functional groups are near the red-colored contours which prefer negative potential in the CoMFA analysis. The hydrophobic group, 3-Br, is located in the hydrophobic pocket formed by Leu13, Pro14, and Tyr15. This binding site corresponds to the sterically favorable CoMFA contours around the substituents at the 3-position.

### Conclusion

A CoMFA analysis was applied to a series of 2-[(aminopropyl)amino]-4(1H)-quinolinone analogues, reported as potent *S. aureus* MetRS inhibitors, for the construction of a predictive QSAR model. The CoMFA model provides a significant correlation between the

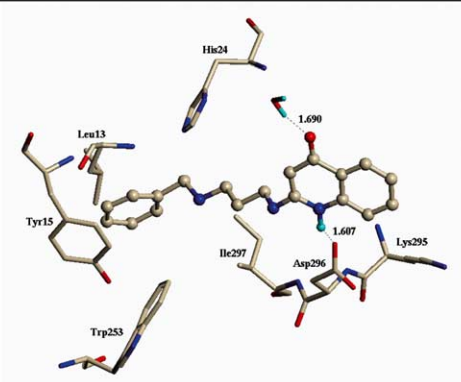
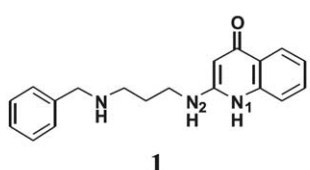
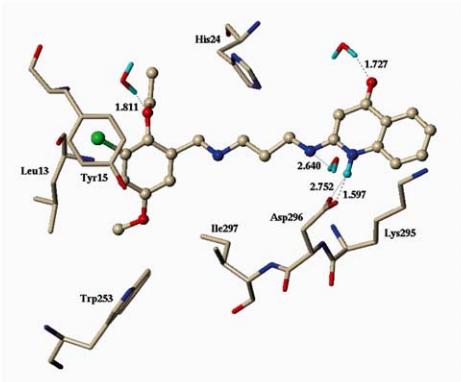
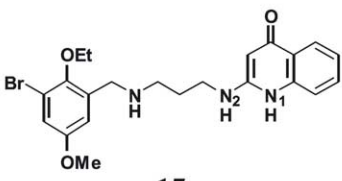
enzyme inhibitory activities ( $IC_{50}$ ) and the CoMFA fields around the MetRS inhibitors. The prediction accuracy of the model was verified with a test set, and the resultant small errors in the prediction proved its value. Further docking studies of a couple of analogues into the binding pocket of *E. coli* MetRS allowed the identification of the MetRS amino acids that form critical interactions with the inhibitors.

### Experimental

#### Data set and molecular structures

The published enzyme inhibitory activities ( $IC_{50}$ ) against a strain of *S. aureus* MetRS were used as the dependent variable (target property) in QSAR study.<sup>13</sup> The  $IC_{50}$  values of seven compounds approaching the observable tight binding limit (3 nM) were excluded in the analysis due to there is little differentiation for the



<i>MetRS-Inhibitor Complex</i>	<i>Hydrogen Bond</i>	<i>Distance (Å)</i>
	 1	
	Asp296.O <sub>d1</sub> ... HN <sub>1</sub> Water.OH ... carbonyl O	1.607 1.690
	 17	
	Asp296.O <sub>d1</sub> ... HN <sub>1</sub>	1.597
	Asp296.O <sub>d2</sub> ... HN <sub>1</sub>	2.752
	Water.OH ... carbonyl O	1.727
	Water.OH ... N <sub>2</sub> H	2.640
	Water.OH ... 2-ethoxy O	1.811

**Figure 4.** Hydrogen bond interactions between the MetRS binding pocket and inhibitors.

most potent compounds. The molecular structures and IC<sub>50</sub> values of the 40 MetRS inhibitors constituting the training set in the QSAR analysis are listed in Table 2. In the regression analysis, the biological activities of the compounds were expressed as the logarithm of 1/IC<sub>50</sub> values, pIC<sub>50</sub>. The larger pIC<sub>50</sub> values imply higher potency for the inhibition of MetRS. The test set of 17 randomly selected MetRS inhibitors is shown in Table 3.

Since experimental information on the three-dimensional structures of this series is not available, the initial structure of each compound was built using the Sybyl molecular modeling program (Tripos, Inc.), and then the geometry was fully optimized using the Tripos force field with the following non-default options (method: conjugate gradient, termination: gradient 0.01 kcal/mol Å, and max iterations: 10,000). The partial atomic charges were calculated by the Gasteiger–Hückel method in the Sybyl program. The Grid search method was used to evaluate the conformational properties of all rotatable functional groups. Each torsion angle was driven from –180 to 180° in 30° increments.

#### CoMFA field and PLS analysis

The calculation of the CoMFA steric and electrostatic fields demands that the molecules should be superimposed in three dimensions. The alignment procedure was performed with the compound **1** as a template

molecule, as shown in Table 2. In this, all of the other molecules were fitted to the template molecule while maintaining their molecular geometry. The CoMFA steric and electrostatic interaction energy fields were generated using an *sp*<sup>3</sup> hybridized carbon atom as a probe with a +1.0 point charge. The energy calculation was performed with 1,350 grid points on a cube (28×19×16 Å, 2.0 Å grid spacing). The energy cutoff for the steric and electrostatic interaction energies was set to 30 kcal/mol.

For the application of a multivariate data classification to the CoMFA models, a partial least square (PLS) analysis was performed using the QSAR module implemented in Sybyl.<sup>17</sup> In the PLS analysis, the QSAR data sets consist of variables with different data ranges. Consequently, prior to the regression analysis the variables are usually scaled in order to give equal influence on the outcome of the PLS analysis. In this study the CoMFA steric and electrostatic fields were scaled using the CoMFA standard scaling option. To determine the predictive *q*<sup>2</sup> and the optimum number of components for the training set, cross-validations were carried out by the 'leave-one-out' procedure. The optimum number of components corresponds to the smallest standard error of prediction. The final 3-D-QSAR model was derived by conventional analysis (non cross-validation) with the optimum number of components.

## Docking of MetRS inhibitors

Among the MetRS inhibitors, the unsubstituted parent compound **1** exhibited poor MetRS inhibition with an  $IC_{50}$  value of 300 nM, while the analogues **17**, **23**, **27**, **29**, **42**, **43** and **53**, which were substituted with more polar and sterically bulky groups, gave significantly improved inhibitory activity to MetRS, with  $IC_{50}$  values <4.0 nM. However, the substitutions with large bulky groups, such as *t*Bu and  $-CO_2Et$ , at the 3- and 5-positions of the aryl moiety showed a dramatic loss of the enzyme inhibition, with  $IC_{50}$  values of 120 and 170 nM, respectively. This observation suggests that the 2-, 3- and 5-positions of the aryl moiety are crucial to interact with the MetRS active site.

To obtain detailed information concerning MetRS inhibitor binding, we examined the binding mode of the MetRS inhibitors. A couple of compounds, **1** ( $IC_{50}$ =300 nM) and **17** ( $IC_{50}$ =3.1 nM), among the MetRS analogues were chosen and docked into the active site of *E. coli* MetRS, by taking the following steps. (1) Scrutiny of the MetRS binding pocket. Recently, the X-ray crystal structure of the *E. coli* MetRS complexed with methionine was solved.<sup>18</sup> The hydrophobic binding pocket consists of 10 amino acids, Ala12, Leu13, Tyr15, Trp253, Ala256, Pro257, Tyr260, Ile297, His301 and Trp305, surrounding the L-methionine ligand. The amine group of the L-methionine is hydrogen bonded to the carboxyl group of Asp52 and the carbonyl oxygen atom of Leu13. The sulfur atom of the ligand forms two hydrogen bonds, with the hydroxyl oxygen atom of Tyr260 and with the amine group of Leu13. As shown in Figure 3a, since the binding pocket is deep and narrow, analogues with large substituents might have difficulty fitting into the pocket of MetRS. (2) Docking studies of selected analogues. Compounds **1** and **17** were each manually docked into the binding pocket proposed by the X-ray crystal structure using the program DOCK implemented in Sybyl 6.5. The initial receptor–ligand complexes were determined using graphical manipulations with continuous energy monitoring. (3) Refinement of receptor–ligand complexes. Hydrogen atoms were added to MetRS, and then the obtained complexes were fully optimized by energy minimization using the Tripos force field. All computational work was done on a Silicon Graphics O<sub>2</sub> R10000 workstation.

## Acknowledgements

This work was supported by a grant (00-PJ1-PG1-CH15-0002) from the Ministry of Health & Welfare, ROK.

## References and Notes

- Public Health Laboratory Service. *Commun. Dis. Rep.* **2001**, *11*, 7.
- Schimmel, P.; Tao, J.; Hill, J. *FASEB J.* **1998**, *12*, 1599.
- Tao, J.; Schimmel, P. *Exp. Invest. Drugs* **2000**, *9*, 1767.
- Ibba, M.; Söll, D. *Annu. Rev. Biochem.* **2000**, *69*, 617.
- De Pouplana, L. R.; Schimmel, P. *Cell. Mol. Life Sci.* **2000**, *57*, 865.
- Hughes, J.; Mellows, G. *Biochem. J.* **1980**, *191*, 209.
- Lee, J.; Kang, M. K.; Chun, M. W.; Jo, Y. J.; Kwak, J. H.; Kim, S. *Bioorg. Med. Chem. Lett.* **1998**, *8*, 3511.
- Lee, J.; Kang, S. U.; Kang, M. K.; Chun, M. W.; Jo, Y. J.; Kwak, J. H.; Kim, S. *Bioorg. Med. Chem. Lett.* **1999**, *9*, 1365.
- Lee, J.; Kang, S. U.; Kim, S. Y.; Kim, S. E.; Kang, M. K.; Jo, Y. J.; Kim, S. *Bioorg. Med. Chem. Lett.* **2001**, *11*, 961.
- Lee, J.; Kang, S. U.; Kim, S. Y.; Kim, S. E.; Jo, Y. J.; Kim, S. *Bioorg. Med. Chem. Lett.* **2001**, *11*, 965.
- Lee, J.; Kim, S. E.; Lee, J. Y.; Kim, S. Y.; Kang, S. U.; Seo, S. H.; Chun, M. W.; Kang, T.; Choi, S. Y.; Kim, H. O. *Bioorg. Med. Chem. Lett.* **2003**, *13*, 1087.
- Jarvest, R. L.; Berge, J. M.; Berry, V.; Boyd, H. F.; Brown, M. J.; Elder, J. S.; Forrest, A. K.; Fosberry, A. P.; Gentry, D. R.; Hibbs, M. J.; Jaworski, D. D.; O'Hanlon, P. J.; Pope, A. J.; Rittenhouse, S.; Sheppard, R. J.; Slater-Radosti, C.; Worby, A. J. *Med. Chem.* **2002**, *45*, 1959.
- Jarvest, R. L.; Berge, J. M.; Brown, M. J.; Brown, P.; Elder, J. S.; Forrest, A. K.; Houge-Frydrych, C. S. V.; O'Hanlon, P. J.; McNair, D. J.; Rittenhouse, S.; Sheppard, R. J. *Bioorg. Med. Chem. Lett.* **2003**, *13*, 665.
- Jarvest, R. L.; Berge, J. M.; Brown, P.; Houge-Frydrych, C. S. V.; O'Hanlon, P. J.; McNair, D. J.; Pope, A. J.; Rittenhouse, S. *Bioorg. Med. Chem. Lett.* **2003**, *13*, 1265.
- Finn, J.; Mattia, K.; Morytko Ram, S.; Yang, Y.; Wu, X.; Mak, E.; Gallant, P.; Keith, D. *Bioorg. Med. Chem. Lett.* **2003**, *13*, 2231.
- Cramer, R. D., III; Patterson, D. E.; Bunce, J. D. *J. Am. Chem. Soc.* **1988**, *110*, 5959.
- Wold, S.; Albano, C.; Dunn, W.; Edlund, U.; Esbensen, K. H.; Geladi, P.; Hellberg, S.; Johansson, E.; Lindberg, W.; Sjöström, M. *Multivariate Data Analysis in Chemistry. In Chemometrics: Mathematics and Statistics in Chemistry, Vol. 138*, Kowalski, B., Ed.; NATO ASI, series C, Reidel Publishing Company, 1984; p 17.
- Serre, L.; Verdon, G.; Choinowski, T.; Hervouet, N.; Risler, J. L.; Zelwer, C. *J. Mol. Biol.* **2001**, *306*, 863.